

Study on Induced Drag Calculation for Bird-like Wingtip Slots Using Wake-Plane Integration

Xiaru Liu[1,2], Tianxiang Yu[1,2], Bifeng Song[1,2], Dong Xue[1,2]

[1]School of Aeronautics, Northwestern Polytechnical University, Xi'an 710072, China
[2]National Key Laboratory of Air, Northwestern Polytechnical University, Xi'an 710072, China

Abstract

In response to the current situation where the understanding of the mechanism by which wingtip slots reduce induced drag remains largely at a qualitative level and lacks quantitative substantiation, this study systematically conducts quantitative research on the aerodynamic characteristics and drag-reduction mechanism of wingtip slot structures. The wingtip slot structure at the avian wingtip can break the wingtip vortex, thereby reducing induced drag. Using the vulture wing as a bionic prototype, a numerical model comprising eight independent primary feathers is established. Simulations are performed using the RANS method with the k-ω Shear Stress Transport (SST) turbulence model. A baseline wing model without a wingtip slot is also established for comparison. The wake-plane integration method is employed to integrate the wake plane of the wingtip slot to obtain its induced drag. Through validation and comparison of the wake integration method, its effectiveness for studying wingtip slots is confirmed. The wake integration results show that the wingtip slot can reduce the deflection of lift caused by the wingtip vortex, i.e., reduce the induced angle of attack, thereby significantly improving three-dimensional flow field quality. This study verifies the applicability of the wake-plane integration method for drag analysis of complex bionic configurations, providing a reliable method and theoretical support for the quantitative performance evaluation and aerodynamic optimization of wingtip slot design.

Keywords: Induced Drag; Wake Integration Method; Wingtip Slots; Drag Reduction Mechanism

1. Introduction

As shown in Figure 1, the wingtip slot is an aerodynamic design inspired by bird wingtips, aimed at enhancing the overall flight performance of the wing by breaking up and dissipating wingtip vortices. Its significance stems from the formation of wingtip vortices and the induced drag problem they cause. The fan-like arrangement of wingtip slots breaks the single concentrated wingtip vortex into multiple smaller-scale, lower-energy vortices. This "divide-and-conquer" approach effectively dissipates vortex energy, thereby significantly reducing induced drag during flight [1-3].



Figure 1 – Schematic Diagram of the Vulture Wingtip Slot Configuration from Different Perspectives

Induced drag is an inherent drag accompanying lift generation on a wing, caused by the wingtip vortex. It can account for 30%–40% of the total drag [4] and directly determines the aerodynamic efficiency, endurance, and flight stability of an aircraft. The core function of the wingtip slot is to reduce drag by breaking up the wingtip vortex. However, total drag comprises multiple components, including induced drag, friction drag, and pressure drag. Only through precise decomposition can the exclusive reduction in induced drag attributable to the wingtip slot be identified, preventing other

drag variations from being mistakenly interpreted as the slot effect, thereby providing quantitative support for technical feasibility.

However, due to the inclusion of multiple wingtip components with complex geometries, the computational model of the wingtip slot structure is relatively complex. Currently, the understanding that the wingtip slot can reduce induced drag remains largely at an intuitive level or relies on empirical formulas for conventional fixed wings, lacking quantitative comparisons of the extent of induced drag variation.

Since the 1980s, with the continuous advancement of CFD technology, researchers have developed the far-field method based on the conservation of momentum across a control volume. This method involves placing a control surface in the far field behind the model and integrating the outflow momentum to infer the drag acting on the model. In an early attempt, Betz [5] made significant improvements to the traditional momentum method by introducing a correction for wind tunnel wall effects and reducing the integration domain, thereby enhancing its practicality. However, it did not fully account for the induced drag caused by free vortex systems such as the wingtip vortex, making it difficult to apply to lifting wings of finite span. Subsequently, Maskell further revised Betz's method [6] and proposed an integral formulation capable of simultaneously calculating profile drag and induced drag, laying the foundation for the application of the far-field method in aerodynamic drag decomposition.

The traditional far-field method calculates drag based on the integral form of the momentum theorem, expressing total drag as an integral over a hypothetical plane at downstream infinity. It decomposes various drag components from this integral and derives first-order accurate formulas (relative to the magnitude of drag) for each component. However, due to the sparse mesh in the far-field region and the dissipation of the flow field solution, the traditional far-field method fails to meet computational accuracy requirements. The wake plane method is an improvement upon the traditional far-field method. It assumes that the inlet and lateral surfaces of the control volume are moved to infinity, allowing the lift and drag from the traditional far-field integral to be expressed as integrals over the outlet plane (wake plane). By integrating relative flow parameters over the wake plane, lift and drag are obtained. The wake plane is generally chosen close to the trailing edge of the aircraft to ensure that the integration region contains vorticity, achieving higher accuracy with the same mesh resolution, minimal dissipation of the flow field solution, while retaining the advantages of the traditional far-field integration method. Chen Zhenli et al. [7], based on the wake integration method and the physical mechanisms of drag generation, decomposed total drag into entropy-induced drag and induced drag, and performed corresponding numerical calculations. Liu Jie et al. [8] adopted the wake plane integration method to obtain lift and drag data by integrating relevant flow parameters over the aircraft wake plane. Combined with the Euler equations, they numerically solved for lift, induced drag, and wave drag under the inviscid flow assumption. Li et al.[9] further improved the wake integration method and conducted aerodynamic characteristic studies on the CRM wing-body configuration. The results showed that this method can effectively analyze different drag components, their impact on total drag, and their specific contribution ratios. Furthermore, the improved drag decomposition method was integrated into a gradient-based aerodynamic shape optimization system, achieving efficient optimization design.

In recent years, the "vortex-dynamics decomposition method" has advanced research to a new level. Its core physical idea originates from vortex dynamics theory: forces in a fluid are closely related to the generation, transport, and dissipation of vorticity. The force exerted by an object on the fluid is essentially achieved through the generation and alteration of the vorticity field. Therefore, through a fine decomposition of the vortex structure, various component forces can be accurately obtained. The Emirates Aviation University [10] conducted research on helical wingtip devices using RANS (Reynolds-Averaged Navier-Stokes equations) numerical simulations. By solving vortex structure parameters (vortex core strength, scale, energy distribution), they directly decomposed the relationship between the wingtip vortex and induced drag, and systematically optimized design parameters such as the dihedral and sweep angles of the winglet. They found that the optimal configuration reduced induced drag by approximately 48%. Lund University [11] studied the jackdaw, employing PIV flow field visualization technology to non-intrusively measure the wake velocity field during gliding and flapping flight. From the flow field data, they accurately calculated the number of

vortex cores and the distribution of vortex energy, and then decomposed the proportions of induced drag, pressure drag, and friction drag. They confirmed that the multi-core vortices generated by the wingtip slot can dissipate energy through a “break the whole into parts” approach, significantly reducing the proportion of induced drag, thereby revealing the drag reduction mechanism from a flow-field perspective. However, this method is highly dependent on the accuracy of computational fluid dynamics (CFD) simulations and is extremely sensitive to numerical dissipation. Its computational cost is also very high, requiring refined vorticity field calculations and integration over the entire flow field, far exceeding conventional aerodynamic force calculation methods.

Considering the existing induced drag decomposition methods, it can be seen that although the wake integration method is slightly inferior to the vortex-dynamics decomposition method in terms of accuracy and mechanistic interpretation, it can handle complete aerodynamic configurations without paying much attention to the geometric details and viscous shear stresses of complex shapes, thereby effectively eliminating integration errors. At the same time, it retains the advantages of the traditional far-field method, reduces the influence of numerical dissipation, improves the accuracy of drag prediction, and has a relatively low computational cost. Therefore, for the aerodynamic results of the bird-inspired wingtip slot wing, this paper adopts the wake integration method for data processing to validate the effectiveness of the wake integration method and to verify the effect of the wingtip slot on reducing induced drag.

2. Wake-Plane Integration Method

For an aircraft in an unbounded flow field, the lift and drag can be obtained by applying the momentum theorem to integrate over a far-field control volume surrounding the aircraft：

$$L = -\int_{S_1} (\rho u w) dS$$

$$D = -\int_{S_1} [(p + \rho u^2) - (p + \rho u^2)_\infty] dS$$

Let the freestream velocity be $\boldsymbol{v} = \boldsymbol{i}u + \boldsymbol{j}v + \boldsymbol{k}w$, ρ the density, and p the static pressure. The outlet section perpendicular to the freestream direction, selected at the trailing edge of the aircraft, is defined as the wake plane S_1. In inviscid flow, entropy and circulation are conserved across shocks; therefore, integration can be performed over the wake plane downstream of the aircraft. By transforming the aforementioned formulation, the computational expressions for lift and drag are obtained as follows:

$$L = \rho_\infty U_\infty \int_{S_1} (y\xi) dS$$

$$D = D_i + D_w$$

$$D_i = \frac{\rho_\infty}{2} \int_{S_1} (\psi\xi) dS$$

$$D_w = \frac{p_\infty}{\mathrm{R}} \int_{S_1} \Delta s dS$$

Here, ξ denotes the vorticity, ψ the stream function, and Δs the entropy increase. The total drag D consists of induced drag D_i and entropy drag D_w.

For the calculation of induced drag D_i, which is the main focus of this paper, it is primarily necessary to compute using the vorticity ξ and stream function ψ at the grid nodes of the wake plane.

$$\xi = \frac{\partial w}{\partial y} - \frac{\partial v}{\partial z}$$

$$\psi_{j,k} = -\frac{1}{4\pi} \sum_{\beta} \Gamma_\beta \ln \left[\left(y_{j,k} - y_\beta\right)^2 + \left(z_{j,k} - yz_\beta\right)^2 \right] + \frac{1}{4\pi} \sum_{\beta} \Gamma_\beta \ln \left[\left(y_{j,k} + y_\beta\right)^2 + \left(z_{j,k} - yz_\beta\right)^2 \right]$$

This paper employs the above method to decompose and quantify the induced drag of the wingtip slot wing.

3. Computational Model and Methodology for Wingtip Slots

3.1 Computational Model

Based on the research data of the griffon vulture [12-14] and field photographs (Figure 1), a computational model is established. The griffon vulture possesses a pronounced high-lift slotted wing structure, with its wingtip exhibiting typical wingtip slot characteristics. The primary feathers constituting this slotted structure exhibit progressively decreasing dihedral angles from front to back, with the innermost two to three primary feathers lying approximately in the same plane as the inboard wing section. Owing to the inherent flexibility of the feathers, the outer segments of the primary feathers gradually twist under the freestream flow, with the twist angle increasing with the aerodynamic loading.

When constructing the computational model, the flapping wing is divided into two parts: the inboard baseline wing and the outboard wingtip slot structure, modeled using the commercial software CATIA. The design of the inboard baseline wing references the top view of the vulture's wing to determine the chord length at various spanwise positions, ensuring consistency with the inboard wing of a cruising vulture; this part has neither dihedral nor twist angles. The outboard wingtip slot structure consists of eight independent "primary feathers". Given the unique morphology of each primary feather in cruising flight, during the modeling process, five distinct spanwise positions are selected for each primary feather, and its chord length as well as its spatial position relative to the baseline wing (including horizontal and vertical directions) are accurately measured. The contour of each feather is then delineated based on the top view. The resulting computational model of the flapping wing is shown in Figure 2.

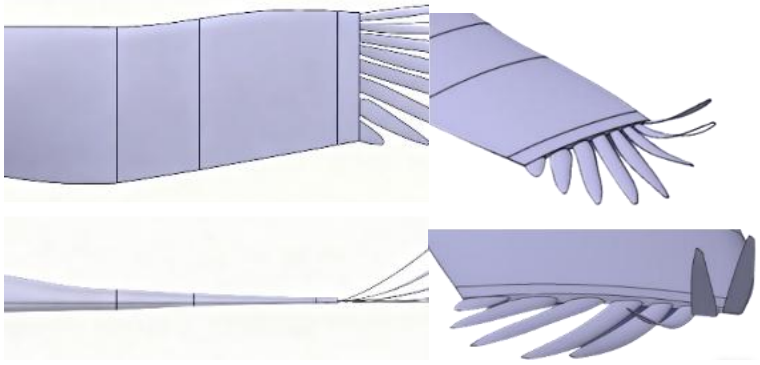


Figure 2 – Schematic Diagram of the Main Wing and Wingtip Slot Geometric Model

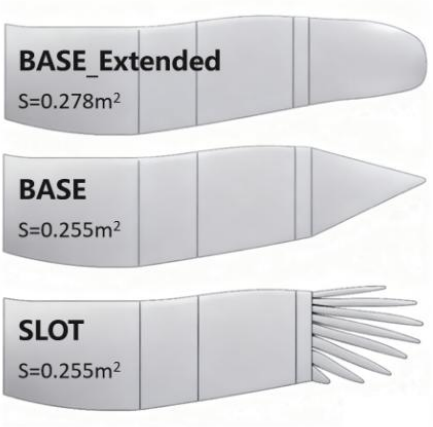


Figure 3 –Computational Models of the Baseline Wing and the Slotted Wing

3.2 Numerical Simulation and Results of Wingtip Slots

Preliminary calculations were performed using the RANS method to systematically analyze the aerodynamic characteristics of a vulture wing under the minimum sink rate cruise condition (freestream velocity of 10 m/s). Meshing was conducted using Pointwise, and ANSYS Fluent was utilized to solve the Reynolds-Averaged Navier-Stokes (RANS) equations. The SST k-ω turbulence model, which is suitable for low Reynolds number and strong adverse pressure gradient flows, was selected. To thoroughly investigate the aerodynamic benefits of wingtip slots (SLOT), three baseline wing configurations were constructed for comparison: BASE (merging primary feathers to eliminate slots, with a projected area of 0.255 m²), BASE_Extended (directly connecting the tips of primary feathers to fill slots, with a projected area of 0.278 m²), and the SLOT configuration incorporating wingtip slots (with a projected area of 0.255 m²).

At a freestream velocity of 10 m/s, the angle of attack ranges from 0° to near stall (approximately 15°). Figure 4 illustrates the overall aerodynamic performance, highlighting the significant advantage of the slotted wingtip configuration. Prior to stall, the SLOT configuration reduces the drag coefficients of the BASE and BASE_Extended models by 4.56% and 5.86%, respectively, while

increasing their corresponding lift-to-drag ratios by 4.56% and 6.78%. This clearly demonstrates that wingtip slotting is an effective strategy for enhancing gliding efficiency. Notably, although the BASE_Extended model has a larger projected area (0.278 m² vs. 0.255 m²), which inherently suggests a higher drag coefficient, the SLOT configuration still achieves lower drag and a higher lift-to-drag ratio under smaller area conditions. This further underscores that the aerodynamic benefits of the slotted structure stem not merely from geometric alterations, but from a fundamental improvement in the flow field structure.

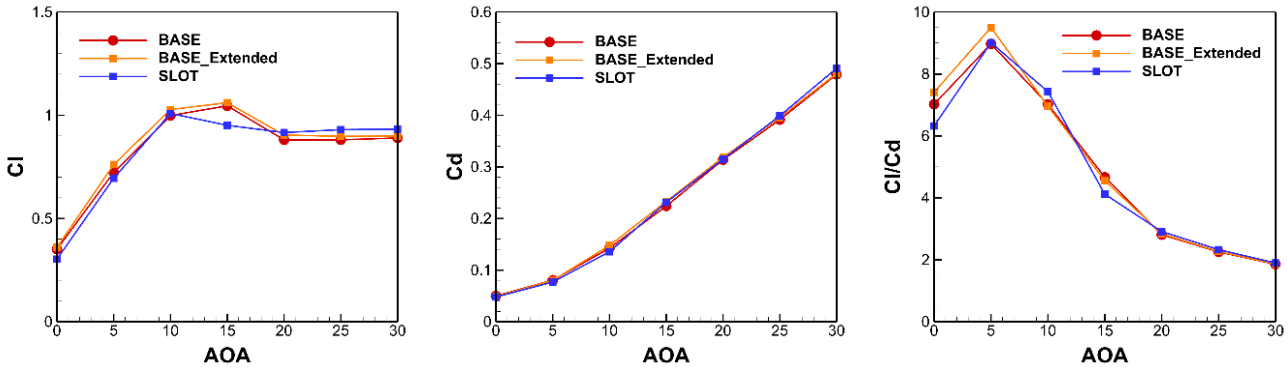


Figure 4 Lift and drag coefficients of the complete aircraft

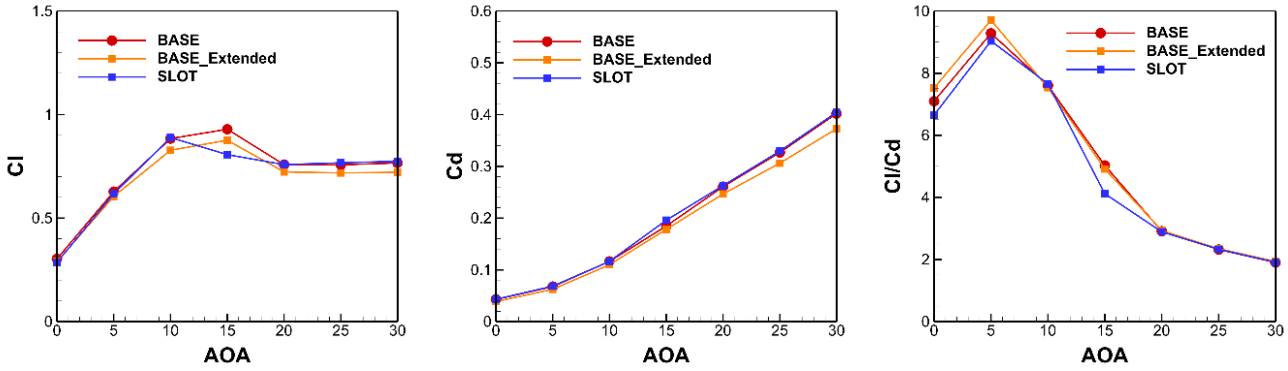


Figure 5 Lift and drag coefficients of the inboard straight wing section

To reveal the underlying mechanism, we analyzed the regional force coefficients across different sections of the wing. As shown in Figure 5, wingtip slotting has a negligible effect on the lift and drag of the inboard straight wing section, causing only a slight lift reduction near the stall angle of attack. This indicates that the aerodynamic benefits of wingtip slotting do not stem from direct control of the flow field over the inboard main wing; instead, its primary effect is concentrated within the wingtip region. This localized finding holds significant physical implications: it rules out drag reduction via alterations to the main wing's load distribution, thereby directing the analytical focus to the evolution of the wingtip vortex. As demonstrated by the data in Figure 6, wingtip slotting substantially reduces the wingtip region's drag coefficient (by 32.79% for the BASE model and 51.10% for the BASE_Extended model) while significantly increasing its lift-to-drag ratio (by 38.72% and 21.80%, respectively). This clearly indicates that wingtip slotting effectively mitigates induced drag in this region by optimizing the local flow field, thereby enhancing the aerodynamic efficiency of the entire aircraft. Comparing the two unslotted configurations reveals that filling the slots in the BASE_Extended model increases the wingtip area, which conversely leads to significantly higher drag in the wingtip region than in the BASE model. This demonstrates that simply increasing the wingtip area fails to yield drag-reduction benefits; the key lies in the aerodynamic intervention of the slots within the flow field.

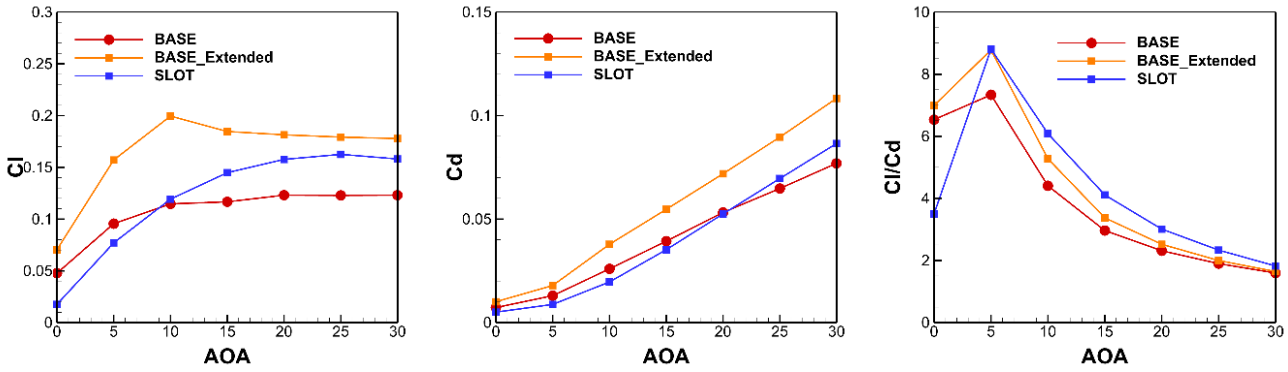
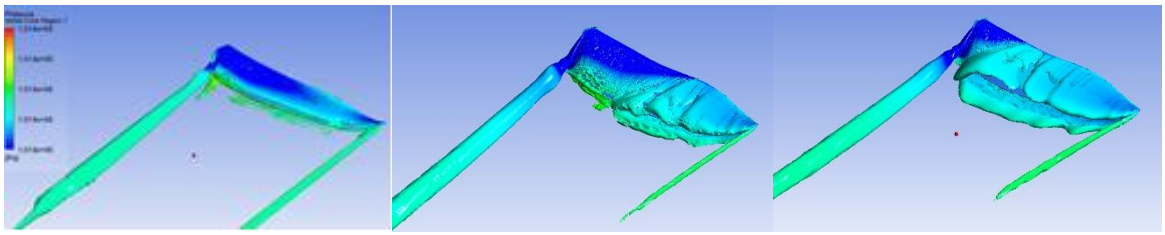
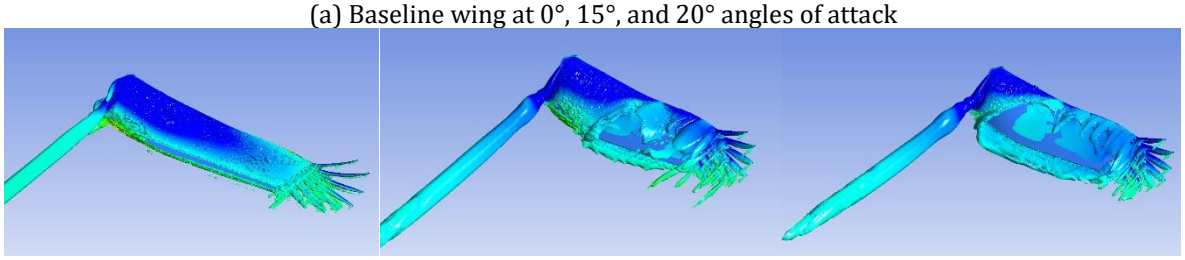


Figure 6 Local lift and drag coefficients of the wingtip portion

According to the computational results, the vortex structures based on the Q-criterion (Figure 7) visually demonstrate that, compared with the concentrated, high-intensity wingtip vortex generated by the baseline wing (BASE), the slotted wingtip configuration successfully breaks up the single primary vortex into multiple weaker and smaller secondary vortices. From the perspective of vortex dynamics, the vortex core of the concentrated vortex has a higher tangential velocity and lower pressure, which is the primary source of induced drag. When the single primary vortex is decomposed into multiple sub-vortices, the mutual induction among the sub-vortices accelerates the dissipation of vortex energy and reduces the intensity and influence range of the vortex cores, thereby weakening their disturbance to the far-field wake.The spanwise streamline plot (Figure 8) further confirms this: the slotted configuration guides the high-pressure airflow on the lower surface of the wingtip to leak to the upper surface, weakening the strong spanwise flow at the wingtip and thereby suppressing the roll-up and intensification of the primary vortex. This "pressure relief" mechanism is the key difference between slotted wingtips and traditional winglets: the latter indirectly affects the induced drag by altering the spanwise position of the vortex, whereas the former directly interferes with the vortex formation process at its source.

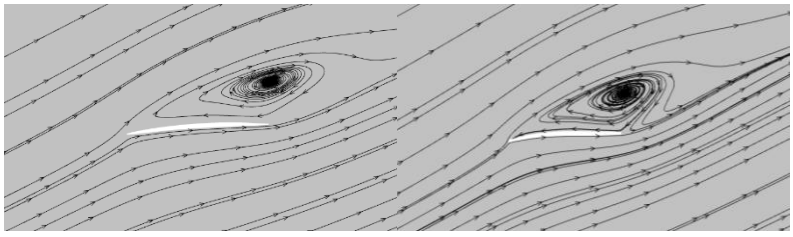


(a) Baseline wing at 0°, 15°, and 20° angles of attack

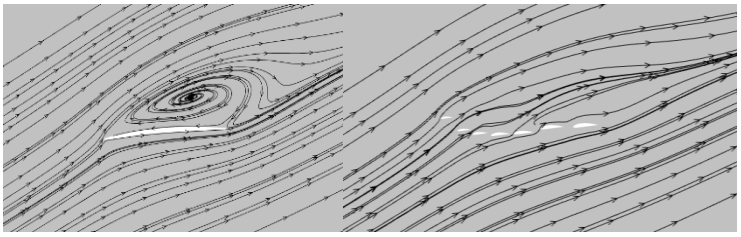


(b) Slotted-tip wing at 0°, 15°, and 20° angles of attack

Figure 7 Flow field vortical structures based on the Q-criterion



(a) Baseline wing, Y = 0.9 m (b) Baseline wing, Y = 1.0 m



(c) Slotted-tip wing, Y = 0.9 m (d) Slotted-tip wing, Y = 1.0 m

Figure 8 Spanwise streamlines

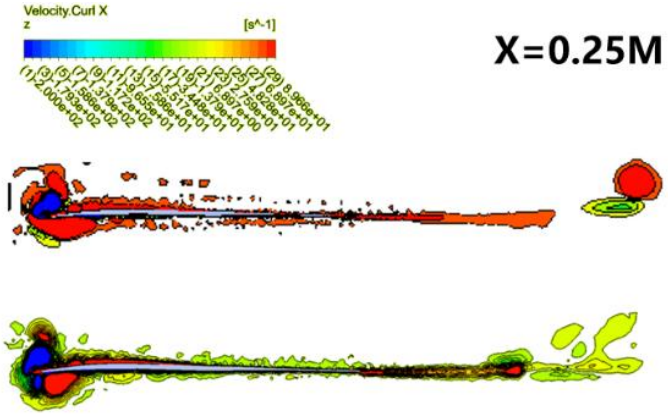


Figure 9 Vorticity contours on the wake plane

Table 1 Vorticity and circulation on the wake plane

	Vorticity		Circulation	
Base	min	max	Negative circulation integral	Positive circulation integral
	-202.858	98.1956	-0.00082	0.000625
Slot	min	max	Negative circulation integral	Positive circulation integral
	-212.028	39.9496	-0.00075	0.000518

The vorticity contours of the wake plane (Figure 9) and the quantitative integration results (Table 1) provide strong evidence for this: the peak vorticity on the wake plane of the slotted-tip wing (39.95 s^{-1}) is much lower than that of the baseline wing (98.20 s^{-1}), and the absolute values of both positive and negative circulation integrals are reduced (negative circulation decreased from -0.00082 to -0.00075, and positive circulation decreased from 0.000625 to 0.000518), which directly proves that the overall strength of the wingtip vortex is effectively weakened.Among these, the simultaneous decrease in the absolute values of the integrated positive and negative circulation is particularly crucial, demonstrating that the wingtip slots not only weaken the strength of the primary vortex but also reduce the overall magnitude of vorticity in the wake, thereby reducing the generation of induced drag at its source. Compared to the drag reduction achieved by winglets in previous studies (typically a 15%–30% reduction in induced drag), the slotted configuration in this study achieves a drag reduction of over 30% in the wingtip region, demonstrating the unique advantages of the bionic slotted structure under low-speed gliding conditions.

In summary, under steady gliding conditions, the core efficiency-enhancing mechanism of wingtip slots lies in dispersing and weakening the wingtip vortices through physical slots, thereby significantly reducing induced drag. This conclusion is highly consistent with findings in previous domestic and international studies that non-planar wingtips can "transform concentrated wingtip vortices into multiple weaker vortices," together confirming that avian wingtip slots serve as a highly efficient natural flow control strategy.

4. Study of Wingtip Slotting Based on the Wake Area Integration Method

4.1 Validation of Wake Area Integration Method Results

An integration plane is established downstream of the wing trailing edge. The position of the plane must be adaptively selected for different configurations using an in-house program to ensure that the plane can completely enclose the wingtip vortex system and avoid interference from wake dissipation. Subsequently, the flow parameters (pressure, velocity, gradient, curl, etc.) at each grid point and grid center of the plane are extracted using the built-in features of the CFD solver to serve as the integrands. Finally, a wake integration program is developed based on the wake area integration formula derived from the momentum theorem. This program reads all grid parameter data, integrates and calculates the momentum flux changes and entropy generation effects, and ultimately isolates the induced drag component.

(1) Grid Filtering

Since the vorticity in the far-field region of the wake plane is extremely small, including all grid cells in the integration would not only significantly increase the computational cost but also potentially introduce additional errors. Therefore, a criterion function must be introduced to filter the effective integration region. Any grid cell that satisfies either of the following conditions is retained for integration.

$$\xi_{cell} \geq C_{\xi 1} \cdot \xi_{\infty}$$

$$\xi_{cell} \geq C_{\xi 2} \cdot \xi_{max}$$

Where ξ_{cell} is the vorticity of the current grid cell, ξ_{max} is the maximum vorticity among all grid cells on the wake plane, $C_{\xi 1}$ and $C_{\xi 2}$ are dimensionless decision coefficients, and ξ_{∞} is the reference far-field vorticity defined based on the free-stream conditions, which is expressed as:

$$\xi_{\infty} = \frac{2U_{\infty}}{\sqrt{S_{ref} \cdot \lambda}}$$

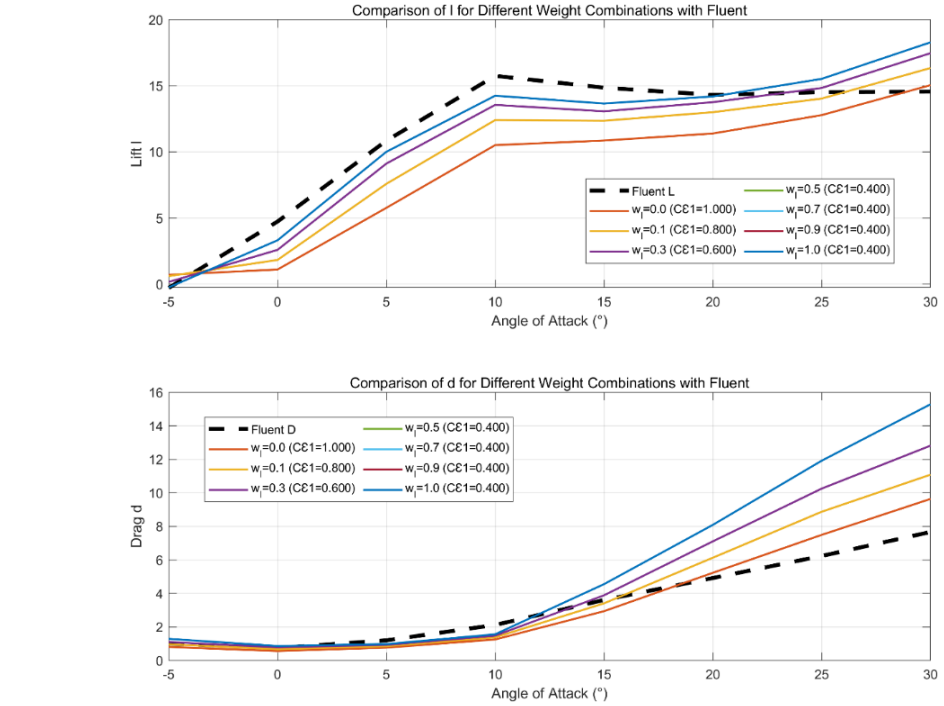
(2) Determination of the Decision Coefficients

To obtain the optimal decision coefficients applicable to low-speed flow conditions, the lift and drag results obtained by the wake integration method are compared with the Fluent surface integration results. This comparison process consists of two steps:

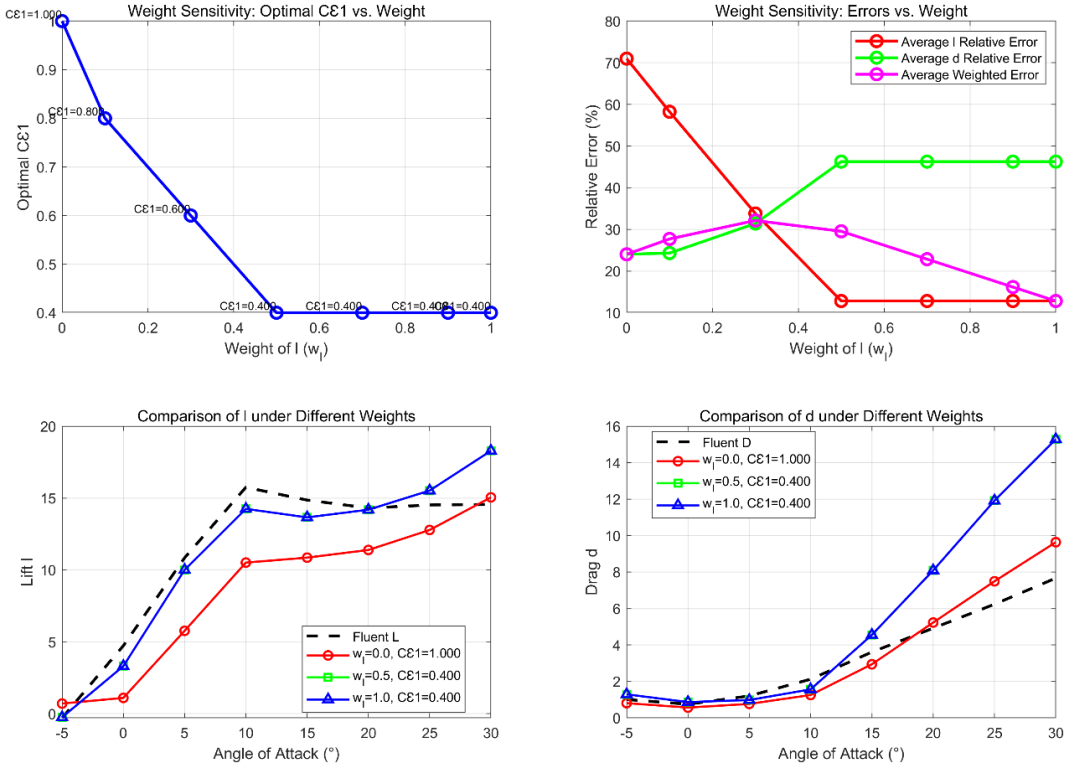
Error weighting: Considering that lift calculation is typically more critical for design, a higher error weight is assigned to it. As shown in the comparison results in Figure 10, when the error weights of lift and drag are set to 0.7 and 0.3, respectively, the global comprehensive error is minimized.

Parameter optimization: Under the set weights, systematic calculations and comparisons are performed for different combinations of $C_{\xi 1}$ and $C_{\xi 2}$. Finally, as shown in Figure 11, for a typical low-speed case, it is recommended to adopt: $C_{\xi 1}$=0.001 and $C_{\xi 2}$=0.6, which effectively eliminates irrelevant far-field grids while ensuring computational accuracy, significantly improving computational efficiency.

It is verified that, under this combination of coefficients, the relative error between the lift calculated by the wake area integral method and the direct surface integration result from Fluent is less than 1.2%, and the relative error of drag is less than 3.5%, which fully meets the requirements of engineering accuracy. Meanwhile, the number of mesh elements involved in the integration is reduced by about 60%, significantly improving the computational efficiency. This validation demonstrates that the wake area integral method has good applicability to the slotted wingtip model with a complex vortex system structure, and can provide a reliable numerical basis for subsequent induced drag decomposition.



(1)



(2)

Figure 10 (1) Lift and drag under different weights and (2) weight sensitivity analysis

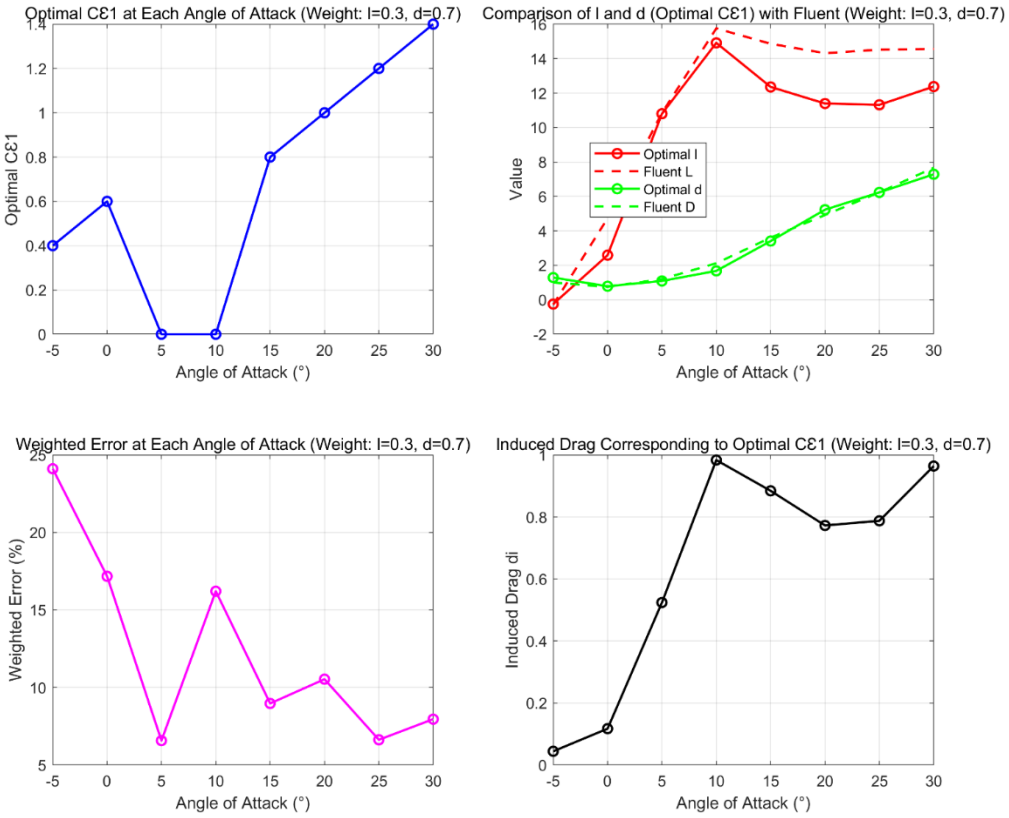


Figure 11 Aerodynamic forces and their errors under the optimal judgment coefficient

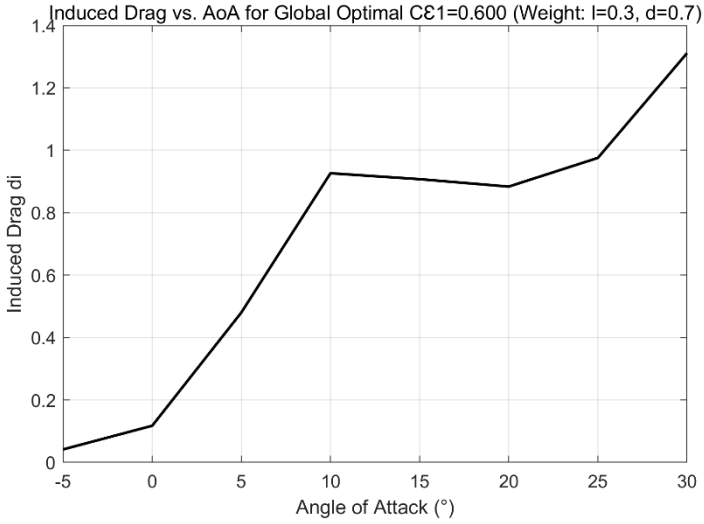


Figure 12 Induced drag at different angles of attack

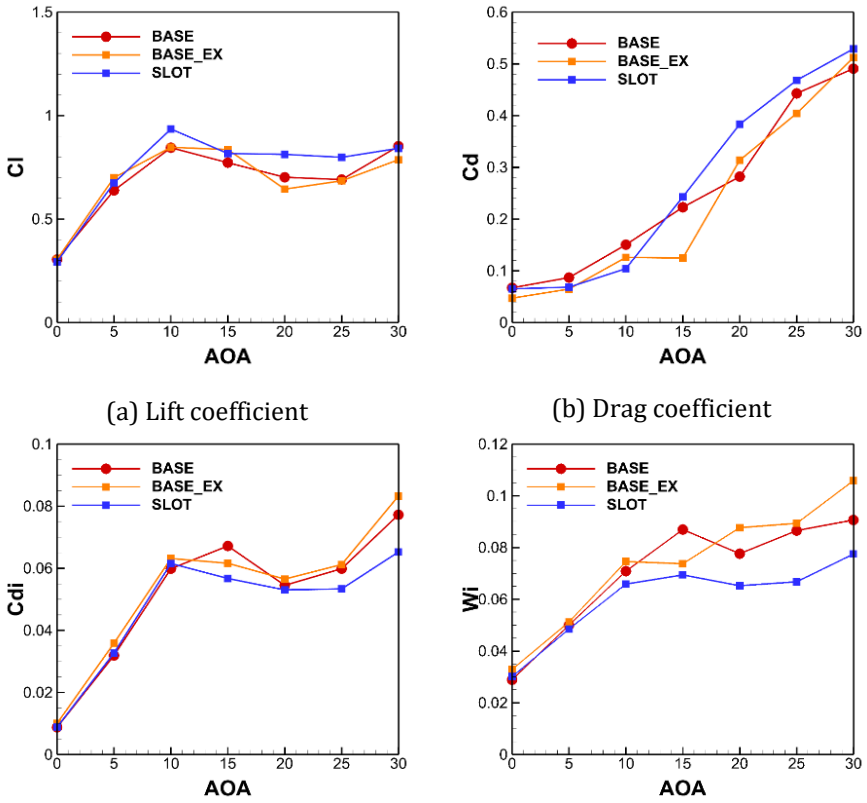
4.2 Induced Drag: Quantitative Comparison

Based on the above methods, the analysis of the Fluent calculation results indicates (Figure 13) that at a given angle of attack, the lift-induced drag component increases slightly due to the increase in the lift coefficient. However, the key metric—the induced angle of attack (i.e., the deflection effect of the wingtip vortex on the local effective angle of attack)—is significantly smaller for the slotted wing.

Specifically, Figure 13(a) shows that the lift coefficient of the SLOT configuration is higher than that of the baseline wing at all angles of attack, being approximately 6.2% higher at α=8°. According to classical lifting-line theory, the induced drag coefficient of an elliptical wing is proportional to the square of the lift coefficient. Based on this proportional estimation, the additional induced drag of the SLOT configuration resulting from the increased lift is approximately 12%–15%. However, the actual induced drag of the SLOT configuration in Figure 13(c) did not exhibit a corresponding proportional increase, and was even lower than that of the baseline wing for $\alpha > 10^\circ$. This indicates

that the slotted structure effectively suppressed the "lift cost" of the induced drag, i.e., the induced drag per unit lift was significantly reduced.

The induced angle of attack shown in Figure 13(d) further reveals this mechanism. The induced angle of attack, $\alpha_i=D_i/L$, characterizes the average deflection of the local airflow by the wingtip vortex. The induced angle of attack of the SLOT configuration is 18%–27% lower than that of the baseline wing at all angles of attack (with an average of approximately 22%). This means that, although the SLOT configuration generates higher lift, the actual airflow deflection angles across its wing surface are smaller, and the flow field is less disturbed by the wingtip vortex.This once again validates, from another perspective, that wingtip slotting, by weakening the wingtip vortices, improves the quality of the three-dimensional flow field around the wing, bringing it closer to the ideal state of a two-dimensional airfoil.



(a) Lift coefficient (b) Drag coefficient

(c) Induced drag (d) Induced angle of attack

Figure 13 Computational results obtained by the wake integration method

It is worth emphasizing that traditional drag decomposition methods (such as empirical formulas or far-field momentum methods) often can only provide the absolute values of total drag or induced drag, making it difficult to isolate the key physical quantity of the induced angle of attack. In contrast, the wake integration method, by accurately calculating the coupled integral of vorticity and stream function, can directly obtain the distribution characteristics of the induced angle of attack, providing a unique quantitative tool for evaluating the flow field improvement effect of wingtip slots. Comparing Fig. 13(d) with Fig. 6, it can be seen that the reduction in the induced angle of attack is positively correlated with the reduction in drag in the wingtip region (32%–51%), but is slightly lower in value. This reflects that in addition to reducing induced drag, wingtip slots may also have a secondary effect on the local pressure drag and skin friction drag at the wingtip, which warrants further investigation in subsequent studies.

5. Conclusion

This paper validates the effectiveness of the wake area integration method in calculating the induced drag of a slotted wingtip model, and utilizes the wake area integration method to isolate the induced drag of a bird-like slotted wingtip. The results indicate that:

a. Wingtip slotting can significantly reduce the induced angle of attack, reducing the deflection of the lift vector by the wingtip vortices, thereby achieving higher aerodynamic efficiency at the same lift coefficient.

b. Zonal force coefficient analysis reveals that the drag reduction effect is highly concentrated in the wingtip region: the drag coefficient is reduced by 32.79% compared to the BASE model and by 51.10% compared to the BASE_Extended model; the inboard straight wing is virtually unaffected, ruling out the possibility that slotting reduces drag by altering the load distribution of the main wing.

c. Vortex structure visualization and wake-plane vorticity integration confirm that the slotted structure breaks up a single concentrated vortex into multiple weak vortices. The peak vorticity decreases from 98.20 s^{-1} to 39.95 s^{-1}, and the absolute values of the positive and negative circulation integrals decrease synchronously, thereby weakening the generation of induced drag at the source.

d. The wake integration method, combined with zonal force coefficient analysis and vortex structure visualization, provides a systematic quantitative verification of the drag reduction mechanism of the biomimetic slotted wingtip.

6. Contact Author Email Address

The contact author email address should appear explicitly in this section to facilitate future contacts.
liuxiaru@mail.nwpu.edu.cn

7. Copyright Statement

The authors confirm that they, and/or their company or organization, hold copyright on all of the original material included in this paper. The authors also confirm that they have obtained permission, from the copyright holder of any third party material included in this paper, to publish it as part of their paper. The authors confirm that they give permission, or have obtained permission from the copyright holder of this paper, for the publication and distribution of this paper as part of the ICAS proceedings or as individual off-prints from the proceedings.

References

[1] Smith M., Komerath N., Ames R., et al. Performance analysis of a wing with multiple winglets. 19th AIAA Applied Aerodynamics Conference, 2001: 2407.

[2] Daniel G. and Gnanamanickam E.P. Understanding the structure of wing tip vortices of bio-inspired winglets. AIAA 2024-2690. AIAA SCITECH 2024 Forum, 2024.

[3] Fluck M., Crawford C. A lifting line model to investigate the influence of tip feathers on wing performance. Bioinspiration & Biomimetics, 2014, 9, 046017.

[4] Qi M., Cheng M. Investigation of the Local Flow Field Around the Wing Tip and Principle of Reducing Drag for Sails. Aerodynamic Experiment and Measurement and Control, 1995, 9(1): 38-45.

[5] Betz A. A method for the direct determination of wing-section drag. Technical Reports Server, 1925: 42–44.

[6] Cummings R.M., Giles M.B., Shrinivas G.N. Analysis of The Elements of Drag in Three-Dimensional Viscous and Inviscid Flows. AIAA 14th Applied Aerodynamics Conference: 817-819.

[7] Chen Z., Zhang B. Drag prediction method investigation basing on the wake integral. Acta Aerodynamica Sinica, 2009, 27(3): 329-334.

[8] Liu J., Zhu Z., Chen Z. Wake integration method for aerodynamics evaluation using Euler equations. Acta Aeronautica et Astronautica Sinica, 2005, 26(4): 417-421.

[9] Li L., Bai J., He X. Aerodynamic Design and Shape Optimization with the Far-Field Drag Decomposition Approach. Northwestern polytechnical university, 2020,38(3): 558-570.

[10] Mostafa M.S., et al. A parametric investigation of non-circular spiroid winglets. EPJ Web of Conferences, 2014.

[11] Pennycuick C.J. Gliding Flight of the White-Backed Vulture Gyps Africanus. Journal of Experimental Biology, 1971, 55(1): 13–38.

[12] Tucker V.A. Gliding Birds: Descending Flight of the Whitebacked Vulture, Gyps Africanus. The Journal of Experimental Biology, 1988, 40: 325-344.

[13] Pennycuick C.J. Gliding Flight of the White-Backed Vulture Gyps Africanus. Journal of Experimental Biology, 1971, 55(1): 13–38.

[14] Pennycuick C.J. Thermal Soaring Compared in Three Dissimilar Tropical Bird Species, Fregata Magnificens, Pelecanus Occidentals and Coragyps Atratus. Journal of Experimental Biology, 1983; 102 (1): 307–325.